scientific reports

Check for updates

OPEN

Integrating metagenomics with metabolomics for gut microbiota and metabolites profiling in acute pancreatitis

Yan Jia[1,2,3], Yuxin Shi[1,2,3], Jie Wang[1,2,3], Honghui Liu[1,2], Yilin Huang[1,2], Hanyue Wang[1,2], Ya Liu[1,2] & Jie Peng[1,2]✉

Acute pancreatitis (AP) is an inflammatory disease of the pancreas. Despite of a steadily increasing in morbidity and mortality, there is still no effective therapy. Gut microbial dysbiosis and its derived-metabolites disorder have been shown to play an important role in the development of AP, however, little is known regarding the crosstalk between gut microbiota and metabolites. In this study, we assessed the alterations in gut microbiota and metabolites by constructing three AP mouse models by means of metagenomic and metabolomic sequencing, and further clarified their relationship by correlation analysis. The results revealed that each model exhibited unique flora and metabolite profiles. KEGG analysis showed that the differential flora and metabolite-enriched pathway functions were correlated with lipid metabolism and amino acid metabolism. Moreover, two core differential bacterial species on *Burkholderiales bacterium* YL45 and *Bifidobacterium pseudolongum* along with eleven differential metabolites appeared to exert certain effects during the course of AP. In conclusion, further exploration of the crosstalk between microbiota and derived metabolites may provide novel insights and strategies into the diagnosis and treatment of AP.

Keywords Acute pancreatitis, Metagenomics, Metabolomic, Gut microbiota

Acute pancreatitis (AP) is a common gastrointestinal disease that contributes to hospitalization in emergency[1]. In recent years, the role of gut microbial dysbiosis in the pathogenesis of AP has received extensive attention[2]. In the occurrence of AP, excessive inflammatory cytokines are released into the bloodstream, and then a series of physiological activities are triggered including gut barrier damage, dysbiosis of gut microbiome, and bacterial translocation[3]. In turn, the bacteria entering the blood through the intestinal wall may influence several organs. There is considerable evidence that bacterial diversity reveals a significant decrease in AP, while the abundance and diversity of gut microbiota are closely related to the gut barrier[4]. Also, with the progression of AP, the imbalance of gut flora has a significant impact on the intestinal barrier function to exacerbate disease[5,6]. In addition, evidence has demonstrated that the severity of AP presents a certain relationship with the composition of gut microbiome[7]. When compared with mild acute pancreatitis (MAP) and moderately severe acute pancreatitis (MSAP) patients, severe acute pancreatitis (SAP) patients have shown a lower abundance of beneficial bacteria such as *Bacteroides*, *Alloprevotella*, *Blautia,* and *Gemella* in fecal samples[8]. With the continuous improvement of advanced sequencing methods such as next-generation sequencing and metagenomics, a more in-depth understanding of the key role of gut microbiota in human health and disease has been observed[9]. As of now, metagenomics has been employed to identify the etiological factors, investigate taxonomic classifications, and determine the underlying mechanisms of AP.

Gut microbiota is involved in the progression of AP by repairing the gut barrier as a result of regulating host metabolism and immune response[10], while gut microbiota-derived metabolites are crucial segments that participate in intestinal-pancreatic axis interactions[11]. It is widely known that gut microbiota elicits superior metabolic activities with the conversion from host and dietary sourced components to a variety of metabolites, some of which take effect not only in the gut but also in other targeted organs far from the intestine through the

[1]Department of Gastroenterology, Xiangya Hospital, Central South University, Changsha 410008, Hunan, China. [2]National Clinical Research Center for Geriatric Disorders, Xiangya Hospital, Central South University, Changsha 410008, Hunan, China. [3]These authors contributed equally: Yan Jia, Yuxin Shi and Jie Wang. ✉email: pengjie2014@csu.edu.cn

circulation, resulting in great influence on physiological and pathological processes[12]. To date, the key role of gut microbiome in AP has been extensively demonstrated, and relative effects of short-chain fatty acids (SCFAs) and bile acid metabolism have also been illustrated[13,14]. However, there is limited knowledge of pertinent literature about non-classical metabolites generated from gut flora. Also, the links between microbiota and metabolites remain complicated and unclear, which needs further exploration. With the critical role of the gut microbiome and its metabolites becomes apparent, identifying new microbial-metabolite combinations and their relationship to AP pathogenesis should be noted.

In this study, we explored the species composition and characteristics of the structure of intestinal microbiota in three AP mouse models. Through metagenomics and untargeted metabolomics analysis, we characterized the bacterial flora of AP and revealed the correlation between gut microbiota and metabolites, which could provide insights into elucidating the underlying mechanisms of gut microbiota and metabolites on the course of AP.

Results

Establishment of three AP mouse models

To assess whether the models were successfully constructed, pancreatic histopathology, cytokines, and serum enzyme levels (lipase and amylase) were evaluated. In the Caerulein group, widening of the lobular septum and cellular gap, edema, vacuolization and necrosis of pancreatic acinar cells, and infiltration of inflammatory cells were observed microscopically in the pancreas. In the Caerulein + LPS group, the pathologic features of the pancreas were similar to those in the Caerulein group and the infiltration of inflammatory cells was more obvious than that in the Caerulein group. As for the L-arginine group, more severe pathological features were found in the microscopy, that is, diffuse necrosis of acinar cells, marked edema of the lobular septum, and infiltration of inflammatory cells (Fig. 1A). The histopathologic scores of the pancreas in the three groups of AP mice were significantly higher than the Control group (Fig. 1B) as well as showed a significant difference of serum amylase, and lipase levels (Fig. 1C,D). Additionally, the number of Ly6G + neutrophils and CD68 macrophages in the pancreatic tissues of AP revealed a highly significant increase compared to the Control group, along with elevation of the serum inflammatory cytokines IL-1β, IL-6, and TNF-α (Fig. 1E–I). The above results indicated the presence of pancreatic injury and systemic inflammatory response in AP mice, suggesting that three AP mouse models were successfully established.

Alterations in intestinal inflammation and barrier function in AP mouse models

Intestinal barrier damage is often accompanied during the onset of AP, and to understand the effects on the gut, HE staining was used to assess the pathology of the colonic mucosa in four groups, which showed normal structure in Control group, with intact and regular intestinal villus structure, and no edema in the interstitium. In the Caerulein, Caerulein + LPS, and L-arginine groups, it demonstrated a relatively intact intestinal epithelium and regular villi arrangement, but the intestinal muscularis was thinned, and the submucosa was dilated and accompanied by lymphoid follicular hyperplasia (Fig. 2A). RT-qPCR was employed to identify the relative mRNA expression of IL-1β, IL-6, and TNF-α in colon tissues. Compared with the Con group, the mRNA levels of pro-inflammatory cytokines were significantly increased in the Caerulein group and Caerulein + LPS group, while there were no significant changes in the L-arginine group (Fig. 2B–D). The integrity of intestinal villi is closely related to intestinal inflammation and barrier function. Therefore, the protein expression levels of ZO-1, Occludin, and Claudin 1 in the colon of four groups were examined by Western Blot, and the results showed that compared with the Control group, the protein levels of ZO-1 and Occludin were significantly reduced in the three AP groups, and concurrently the protein level of Claudin 1 was also demonstrated a highly significant reduction in the Caerulein + LPS group (Fig. 2E,F). Based on these findings, the intestinal mucosal barrier function of mice was damaged to different degrees during the development of AP.

Analysis of gut microbiome diversity

Alpha diversity specifically refers to the diversity and abundance of species in a community and is mostly used to assess the differences in species diversity within a colony. Results demonstrated (Fig. 3A–C) that in comparison with the Control group, the Chao 1 index of the L-arginine group decreased significantly, the Shannon index of the Caerulein and L-arginine groups revealed a highly significant reduction, and along with a marked increase of Simpson index in the Caerulein + LPS group ($P < 0.05$). Beta diversity reflects the differences in the composition of the species diversity in different communities, which are always measured according to PCoA to assess the sample distance between two groups to reflect the structure of the gut microbiota. It provided an overview of the gut microbiome that Caerulein, Caerulein + LPS, and L-arginine groups could be clearly distinguished from the Control group (Fig. 3D–F), indicating that all three AP models differed from the Control group ($P < 0.05$). ANOSIM analysis is a statistical method to analyze the similarity between groups of high-dimensional data. The results of this study are shown in Fig. 3G–I. Separate comparisons between three AP models and Control group were performed with the R values of 0.997, 0.381, and 0.407, accompanied by the P values of 0.003, 0.001, and 0.003, indicating that all three AP models displayed a difference with the Control group.

Characterization of the species composition of the gut microbiota in AP and enrichment analysis of related functional genes

Characterizing the abundance of gut microbiota at different annotation levels in a relative quantitative perspective, when compared with the Control group, the results showed the abundance of the top ten phyla in different groups, as shown in Fig. 4A. Analysis of the composition of microbiomes (ANCOM) revealed that *Proteobacteria* was upregulated in the three AP models along with an increase in *Bacteroidetes* in the Caerulein group and L-arginine group. As for the Caerulein group, *Firmicutes* demonstrated a significant downregulation, while the

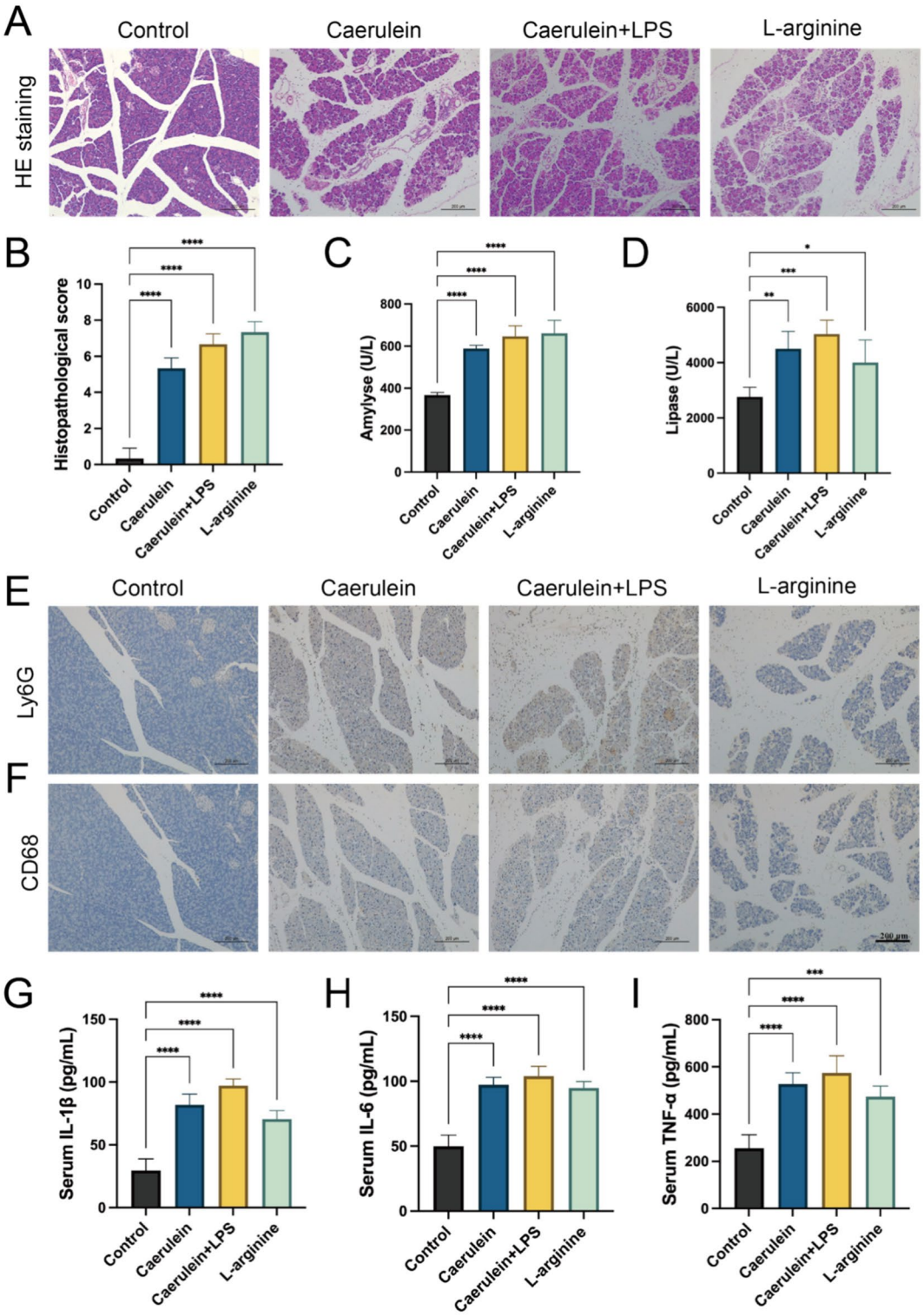

Fig. 1. Establishment of three AP mouse models. (**A**) HE staining of histopathological images of pancreatic tissues among the four groups. (**B**) Histopathological scores of pancreatic tissues in different groups. (**C**,**D**) Serum amylase and lipase levels. (**E**,**F**) Immunohistochemical pictures of pancreatic tissues among the four groups with Ly6G and CD68. (**G**–**I**) Serum levels of inflammatory cytokines IL-1β, IL-6, and TNF-α in different groups. N = 6 mice. Data are presented as mean ± SD. AP model groups were compared to the Control group, *P < 0.05; **P < 0.01; ***P < 0.001; ****P < 0.0001.

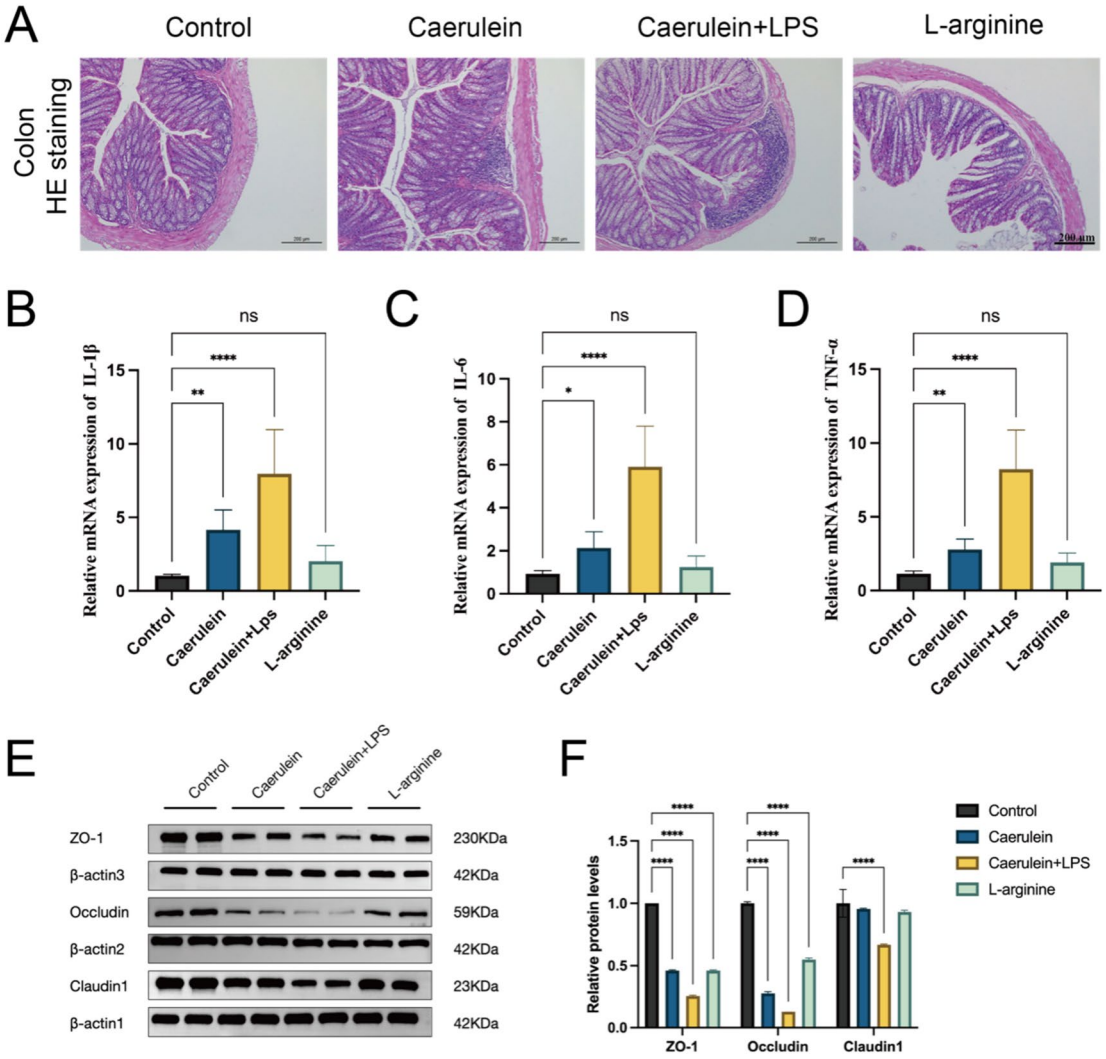

Fig. 2. Comparison of intestinal barrier function in three AP mouse models. (**A**) HE staining of pathological images of colon tissues among the four groups. (**B**–**D**) Relative mRNA levels of IL-1β, IL-6, and TNF-α in colon tissues. (**E**, **F**) Protein expression levels of ZO-1, Occludin, and Claudin 1 in colon tissues. The uncropped blots are shown in the supplementary information file. N = 6 mice. Data are presented as mean ± SD. Statistically significant differences were marked with: *P < 0.05; **P < 0.01; ***P < 0.001; ****P < 0.0001 when compared with Control group.

contrary tendency appeared in L-arginine group (Fig. S1, Table S1). Then, the composition of the top ten species was analyzed, and the results are shown in Fig. 4B as described by differences in the species composition among the four groups. Furthermore, the histograms of the distribution of linear discriminant analysis (LDA) values obtained from the LEfSe analysis (Fig. 4C–E, LDA > 3.0 as the screening criterion) also revealed differences in microbial abundance between the Control group and the AP models. Collectively, these results suggested that species composition at the phylum and species levels could be influenced in AP models. KEGG analysis was utilized to explore the main signaling pathways involved of the differential functional genes, and after that found metabolism (i.e., amino acids, carbohydrates, and lipids) and information processing pathways were involved (Fig. 4F–H)[15–17].

Multivariate statistical analysis of serum metabolites in AP

To analyze the differences in metabolic profiles between groups, multivariate statistical analysis was used to reduce the dimensionality of the complex data. PCA analysis showed that the samples of the Caerulein group, the Caerulein + LPS group, and the L-arginine group could be clearly differentiated from those of the Control group (Fig. S2A-C), which suggested that there existed enlarged differences between Control and AP groups and a large number of metabolites were differentially expressed with an indirect description of successful model construction in this study. Then, to further screen the differential metabolites between the Control group and the AP groups, the results were analyzed with the aid of OPLS-DA shown in Fig. S2D-F, which showed a clear separation between the Control group and the AP groups, likewise indicating that there were significant differences of the metabolites in the AP groups compared with the Control group. Subsequently, OPLS-DA model

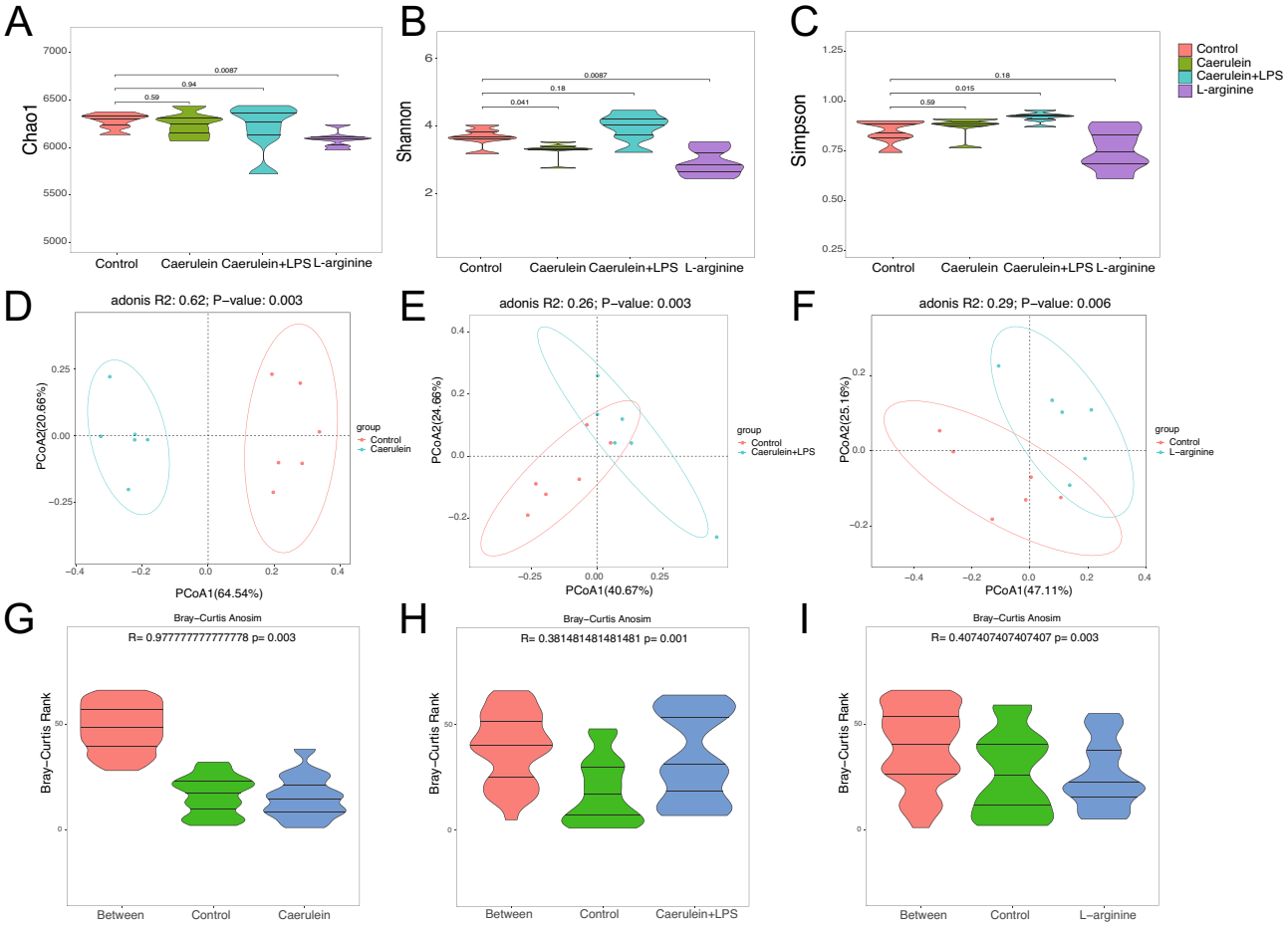

Fig. 3. Diversity analysis of gut microbiota in three AP models. (**A**) Chao 1 index. (**B**) Shannon index. (**C**) Simpson index. (**D**–**F**) PCoA plots showed statistically significant differences between the Control and AP groups respectively. (**G**–**I**) ANOSIM plots showed statistically significant differences between the Control and AP groups. N = 6 mice.

R2X (cum), R2Y (cum), and Q2 (cum) scores were further calculated with the result of 0.347, 0.994, and 0.773 within Caerulein group in contrast to Control group, in the meanwhile, it showed a calculation of 0.437, 0.99 and 0.917 in Caerulein + LPS group, followed by 0.336, 0.967 and 0.381 in L-arginine group. Also, the accuracy of the OPLS-DA was assessed utilizing the 200 response permutation testing (Fig. S2G–I).

Analysis of differential metabolites

In this study, a total of 512 metabolites were identified and classified. Excluding the classification of others, the top 5 substances were lipids and lipid-like molecules (192, 37.5%), organic acids and derivatives (95, 18.6%), organoheterocyclic compounds (65, 12.7%), organic oxygen compounds (43, 8.4%), and benzenoids (19, 3.7%) (Fig. 5A). Volcano plots were used to show the trend of the expression of all detectable substances in the Control group versus the AP model groups, with VIP > 1.0 and P < 0.05 as the differential metabolite screening thresholds, showing a large number of differential metabolites presented in all three AP model groups compared with the Control group (Fig. 5B–D). Then, pathway enrichment analysis of potential biomarkers and screening of pathways with impact values greater than 0 were performed using the MetaboAnalyst system. As shown in Fig. 5E–G, the primary pathways included arginine and proline metabolism, cysteine and methionine metabolism, linoleic acid metabolism, valine, leucine, and isoleucine biosynthesis, glycine, serine, and threonine metabolism, and histidine metabolism, tryptophan metabolism, and biosynthesis of unsaturated fatty acids. All of these pathways played an important role in a variety of physiological functions, suggesting that metabolites were involved in the occurrence of AP by affecting normal physiological functions.

Microbiota-metabolite correlation analysis

To clarify the relationship between metabolites and gut microbiota, spearman's correlation analysis was performed on the differential flora (LDA > 3.0 as the screening criterion) and metabolites in the AP model groups, and the absolute value of the correlation coefficient > 0.8 was further used as the screening criterion to construct the intestinal microflora-metabolite correlation network. The results showed (Fig. 6A–C) that in the Caerulein group, 15 differential strains such as *Bacteroides thetaiotaomicron* were identified as the core strains, and 19

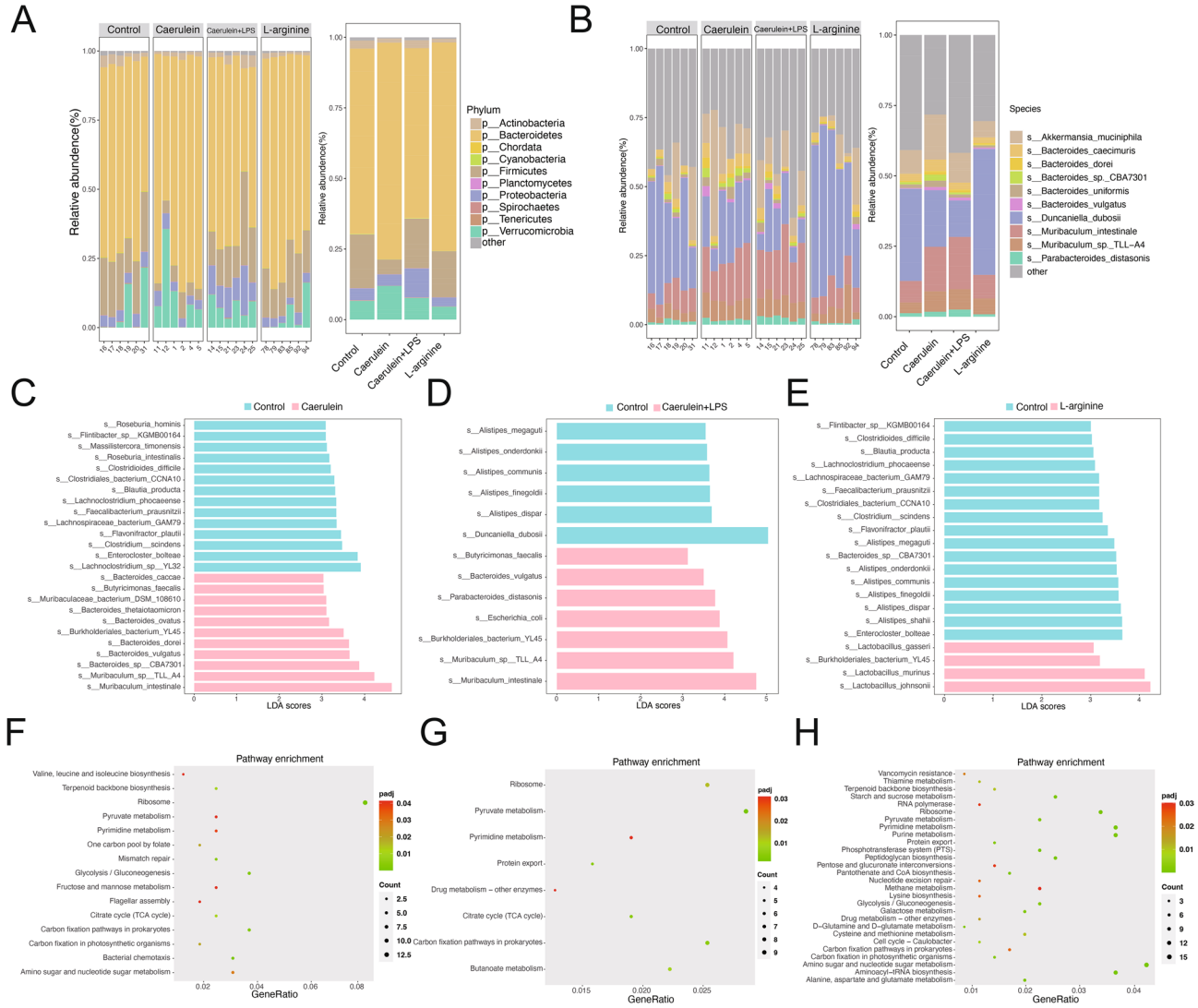

Fig. 4. Compositional structure of gut flora and KEGG pathway enrichment analysis. (**A**,**B**) Relative abundance of the top ten gut microbiota at the phylum and species levels. (**C**–**E**) LefSe analysis showed predominant gut microbiota. (**F**–**H**) KEGG enrichment pathways in AP mouse models in comparison with the Control group. N = 6 mice.

differential metabolites such as MethylIndole-3-acetate were determined as the core metabolites. As for Caerulein + LPS group, 6 differential bacteria including *Alistipes communis*, and 17 differential metabolites such as 3-Methylglutarylcarnitine were core strains and metabolites respectively. Also in the L-arginine group, 10 differential flora including *Alistipes onderdonkii*, and 18 differential metabolites such as 2-Hydroxystearic acid were recognized as core intestinal bacteria and metabolites. Then, the differential strains of the three AP model groups (LDA > 2.0 was used as the screening criterion) were taken as intersections, and the Venn plots (Fig. 6D) showed that *Burkholderiales bacterium* YL45 and *Bifidobacterium pseudolongum* differed significantly among the three model groups, and presented an increasing tendency in all AP mouse models. Similarly, a total of 16 metabolites were significantly different in the three models (Fig. 6E), among which 14 metabolites changed in the same direction (including 7 up-regulated and 7 down-regulated), and we then carried out a spearman correlation analysis of the two differential strains with the 14 differential metabolites, results showed that the two strains were correlated with 11 differential metabolites (Fig. 6F).

Discussion

AP is characterized as an inflammatory response caused by pancreatic enzyme activation with multiple etiologies, which leads to autodigestion of pancreatic tissues and then secondary edema, hemorrhage, and necrosis. Currently, the common modeling methods of AP include administration of Caerulein, Caerulein + LPS, and L-arginine. In previous studies, researchers focused on convenience for operation, reproducibility, and clinical relevance of these 3 models, in order to provide guidance for choosing the appropriate AP model[18–20]. However, to date, the explorations remain single omics or single models with the difficulty to completely summarize the

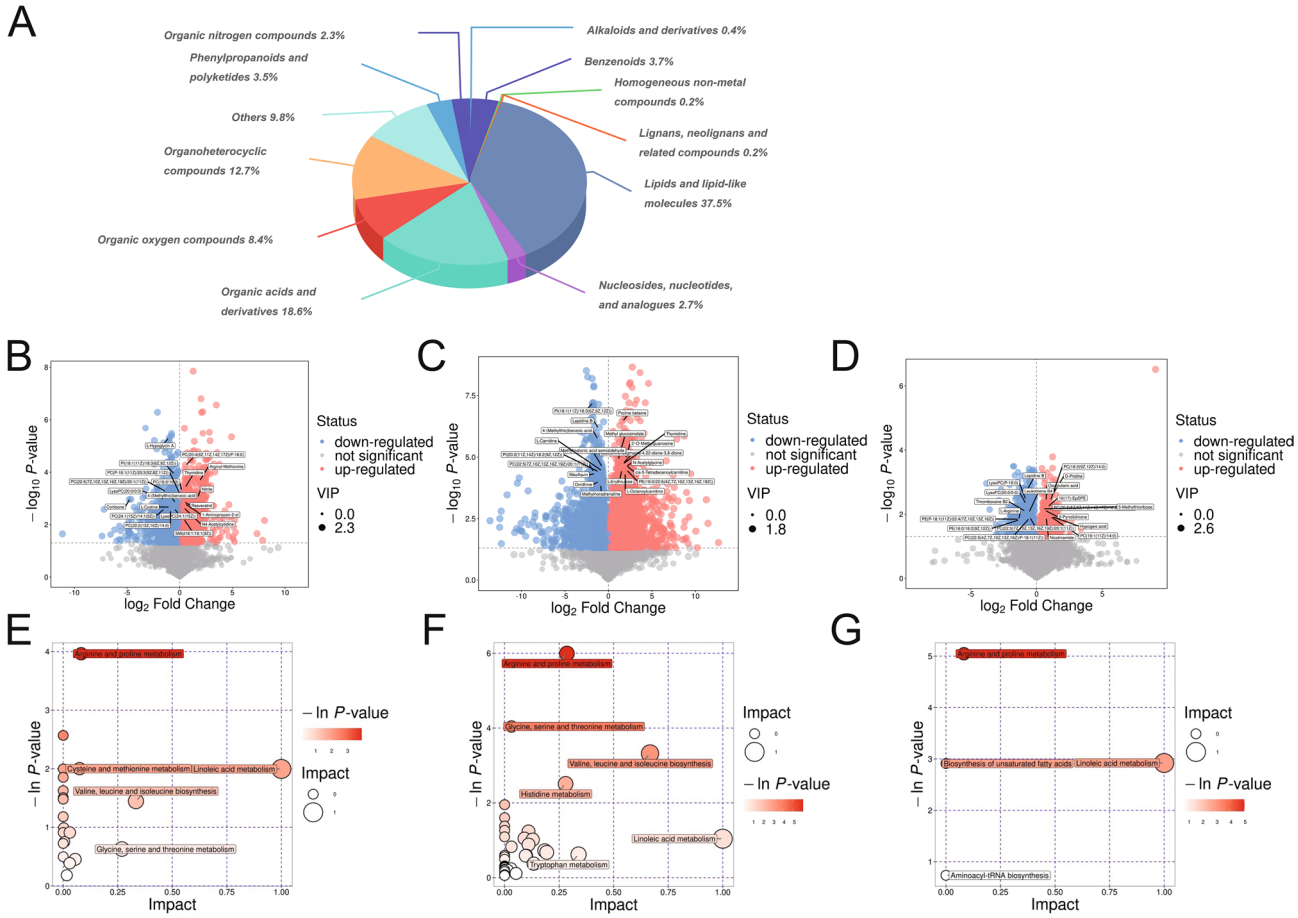

Fig. 5. Differential metabolite analysis and metabolic pathway analysis. (**A**) Pie chart showed the categories of the different metabolites. (**B**–**D**) Volcano plots showed differential metabolites and VIP values in the Control and AP groups. (**E**–**G**) Bubble plots of significantly differential metabolite pathway analysis in the Control and AP groups. N = 6 mice.

clinical phenotype of AP because of the limitation of animal models. Thus, further studies need to concentrate on multi-omics and models to provide a perfect evidence chain for clinical research.

We constructed three AP mouse models in this study and found that all of them showed pancreatic and intestinal barrier injury. In the Caerulein and Caerulein + LPS group, we found consistent alterations in H&E phenotype and other biochemical markers, however, it was interesting that the L-arginine group presented inconsistent results. In the previous studies, Zhang et al. found that the amylase and lipase of L-arginine-induced AP model were elevated at 6 h, reached the peak at 12 h, and then gradually decreased[21]. Also, Hegyi et al. found that the IL-1β levels increased significantly at 12 h after L-arginine injection, peaked at 24 h, and decreased thereafter[22]. In this study, the time point of observation was considered as 72 h, therefore the relevant indexes declined in consistency with previous results. However, other literature has also shown that pancreatic injury (including amylase and lipase levels) is the severest in the L-arginine-induced AP model at 72 h[23]. This inconsistency remains controversial which needs to collect relevant samples at different time points of the model in subsequent experiments to determine the exact trend of the changes. As for the intestinal barrier injury, it was manifested in pathological damage to the intestinal mucosa and down-regulation of tight junction protein levels. Studies have shown that intestinal barrier damage is one of the major complications of AP, as revealed in a meta-analysis study, 59% of AP patients have found gut barrier dysfunction[6]. In addition, another study showed that bacterial DNA representing gut microbiota could be detected in the blood of 68.8% of patients with AP, suggesting that gut microbiota can be translocated to the bloodstream through the damaged gut barrier in AP[24]. Also, the translocation of gut flora can further lead to pancreatic tissue necrosis and infection, thus triggering SIRS and MODS[25], which is closely related to the high mortality of SAP patients.

In this study, we observed the alteration of gut microbiome in three AP mouse models and found good general agreement with previous clinical and animal studies in the variation tendency of *Firmicutes*, *Bacteroidetes*, and *Proteobacteria* at the phylum level, which reflected the reliability and reproducibility of metagenomics sequencing as well as the potency of inference to clinical research[26–28]. Also, an elevation of the abundance of *Burkholderiales bacterium* YL45 and *Bifidobacterium pseudolongum* was captured in three AP models through the comparison at the species level, indicating that they may exert crucial role in the progression of AP, while the specific actions need to be further explored. As an unclassified member of *phylum Proteobacteria* and *genus*

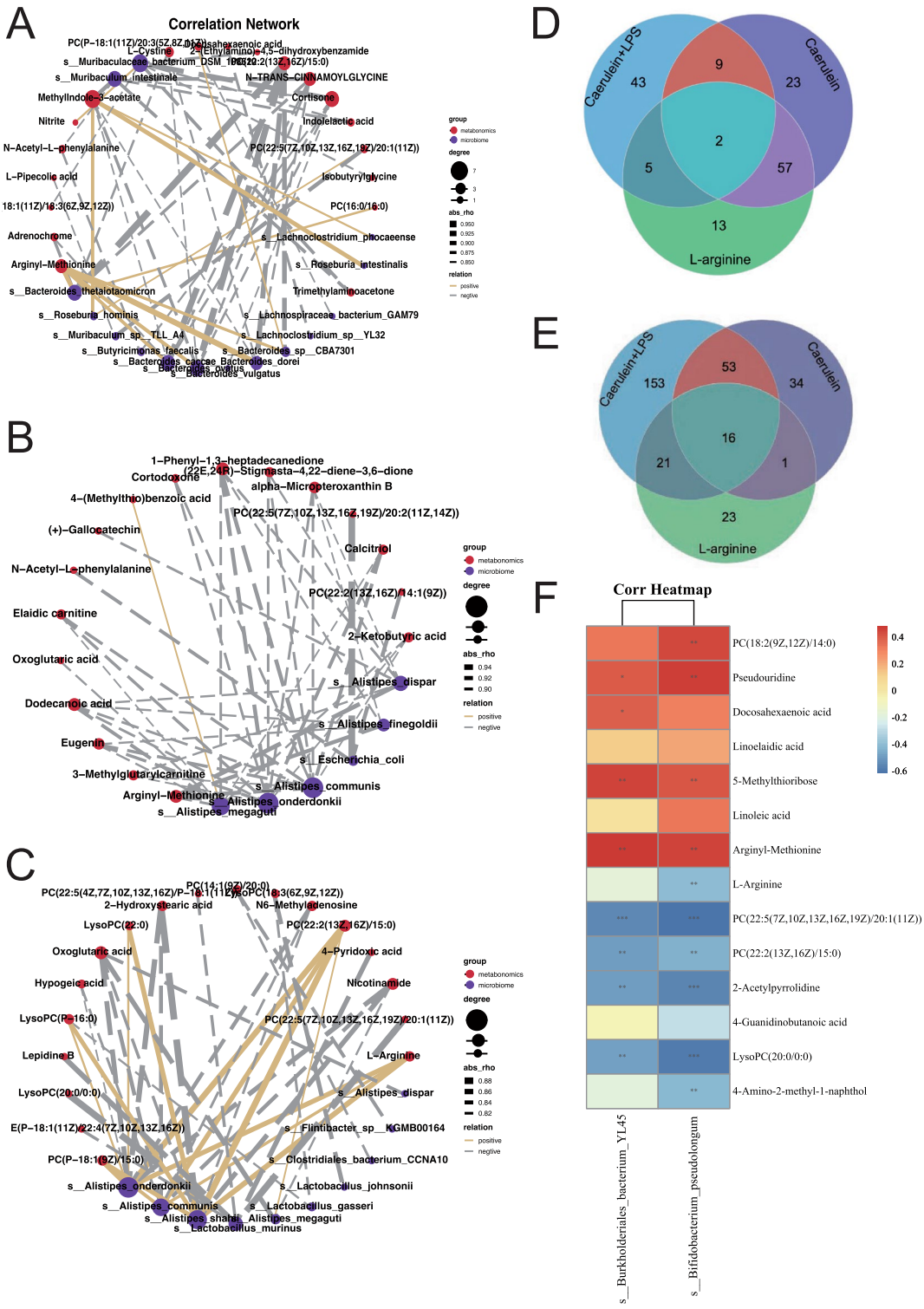

Fig. 6. Microbiota-metabolite interactions. (**A**–**C**) Network diagram of a differential microbiota-metabolite correlation between Control and AP groups. (**D**–**E**) Venn plots demonstrated the intersection of the differential strains and metabolites in three AP mouse models. (**F**) Heatmap of the correlation between common differential strains and metabolites. N = 6 mice. Significant level was marked with *P < 0.05; **P < 0.01; ***P < 0.001; ****P < 0.0001.

Burkholderiales, *Burkholderiales bacterium* YL45 has demonstrated persistent existence and occupied a dominant position in active inflammatory bowel disease[29]. Concurrently, another study found its effect on disease deterioration by ileum colonization, suggesting the involvement in inflammatory diseases[30,31]. *Bifidobacterium pseudolongum* belongs to the *genus Bifidobacterium*, which presents beneficial efficiency on the elimination of pathogens and immune regulation[32]. As shown in non-alcoholic fatty liver disease-associated hepatocellular carcinoma, *Bifidobacterium pseudolongum* could remodel the composition of gut microbiome and improve the gut barrier function to prevent occurrence of disease[32]. Moreover, gut barrier damage was detected to be alleviated in mice with colitis by modulating PPARγ/STAT3 pathway and gut microbiome composition, restoring antioxidant enzymes' activities, along with suppressing the release of proinflammatory cytokines[33]. However, we observed a high abundance of *Bifidobacterium pseudolongum* in three AP models in the current study, indicating its side effects on AP. Likewise, it was found that the abundance of *Bifidobacterium pseudolongum* was increased with a positive correlation to cytokines in influenza[34]. In a comprehensive consideration, this surprising result might be attributed to the heterogeneity of reaction towards diseases, that is specifically microbial-mediated protection of the host.

As a result of metabolomics analysis, a total of 14 metabolites existed differences in three AP models and manifested a consistent variation tendency. Docosahexaenoic acid (DHA) is an omega-3 polyunsaturated fatty acid that has been widely explored in the prevention and treatment of many diseases due to its antioxidant and anti-inflammatory functions. Besides, relevant animal and cellular studies have found a positive effect of DHA in AP at present[35], however, this effect is closely related to the concentration with relatively high concentrations of DHA inducing Ca^{2+}-mediated activation of protein kinase C (PKC) isoforms (PKC-α, PKC-δ, PKC-ε, and PKC-ζ) and zymogens in pancreatic acinar cells, which promotes the progression of AP[36]. In this study, AP-related metabolites were mainly involved in glycerophospholipid metabolism pathway (PC (22:5 (7Z, 10Z, 13Z, 16Z, 19Z)/20:1 (11Z)), PC (22:2 (13Z,16Z)/15:0), LysoPC (20:0/0:0), PC (18:2 (9Z,12Z)/14:0)) with a close relationship to the development of diseases. Phosphatidylcholine (PC) is an important biomolecule whose molecular structure contains a polar phosphatidylcholine head and two nonpolar fatty acid hydrocarbon chains. As a category of the core phosphoglycerolipid metabolites, they have been identified as a key player in the composition of mammalian cell membranes and are closely associated with a variety of physiological processes[37,38]. When it comes to Lysophosphatidylcholine (LPC), a major component of oxidatively damaged low-density lipoproteins, it shows strong bactericidal and anti-inflammatory effects. In infectious diseases such as sepsis, peritonitis, and pneumonia, LPC inhibits the inflammatory response by suppressing the production of inflammatory mediators and increasing the levels of anti-inflammatory factors[39,40]. Additionally, Linoelaidic acid (LA) is classified as a major component of LDL and an essential fatty acid, which can be oxidized by circulating endogenous enzymes and reactive oxygen. It has been reported that levels of LA and arachidonic acid were significantly elevated in AP patients[41], and similarly, LA produced from lipolysis was observed to be lipotoxic in the SAP mouse model, which could contribute to renal tubular injury[42]. The above differential metabolites in AP have been widely explored and are expected to be applied in the diagnosis and treatment of AP, whereas their specific regulatory mechanisms and subsequent clinical applications remain to be further investigated.

We performed function analysis based on the gut microbiome-related differential genes between the Control group and the three AP groups. It was surprising to find a highly consistent result with that of serum metabolomics, to be specific, it was mainly associated with several signaling pathways, such as metabolism (lipid metabolism, amino acid metabolism) and information processing. Disorders of amino acid metabolism are involved in a variety of disease processes including AP, and several recent studies have shown that targeted amino acid supplementation contributes to the remission of AP, in which the interaction mechanism involves anti-inflammatory, antioxidant, etc[43,44]. Amino acid metabolism may be an important therapeutic target of AP. Specifically, if we found a certain amino acid was decreased/increased in AP, whatever human or mice samples, the corresponding supplementation or decrease of this amino acid may relieve AP. In the present study, we identified multiple alterations in amino acid metabolism. Valine, leucine, and isoleucine are the main components of branched-chain amino acids (BCAAs) with an elevated expression in necrotizing AP models[45], and their production of succinyl coenzyme A and acetyl coenzyme A can enter the tricarboxylic acid cycle or through the process of gluconeogenesis to generate energy to meet the high catabolic state of AP[46]. However, the specific actions and in-depth mechanisms targeting the amino acids need to be further explored. Evidence has existed to support the role of enhancing the expression of tight junction proteins, and mucosal immune function of BCAAs, together with being potential biomarkers for a variety of diseases. In the present study, in contrast, both metagenomic and metabolomic analyses revealed that AP was linked with the synthesis of BCAAs, prompting the possibility of the utilization as biomarkers and therapeutic targets for AP[47]. Regarded as significant parts of protein synthesis, methionine and cysteine are engaged in the regulation of sulfur metabolism as well as glutathione synthesis[48]. During the development of AP, methionine and cysteine metabolism is dysregulated owing to dysregulation of trans-sulfur regulation mediated by nitration of cystathionine-β-synthase, resulting in a rapid depletion along with a significant reduction in glutathione levels[49], whereas glutathione depletion has determined to be an accordant feature of the progression from MAP to SAP which can be attributed to aggravating oxidative stress and impaired upstream and downstream amino acids biosynthesis[50]. Arginine metabolism promotes NO production in the early stages of acute inflammation, and the combined impairment of arginine and NO metabolism has the chance to lead to the disruption of intestinal barrier function and progression of inflammation[51]. Simultaneously, a succession of catabolic processes take place including catabolizing into ornithine and urea under the action of arginase, and then ornithine is further decarboxylated to polyamines and proline[52]. Proline has been discovered to improve human immune defense and resistance to foreign antigens and pathogens through gut-associated lymphoid tissues, while polyamines can regulate the integrity of the intestinal epithelial barrier by controlling the expression of tight junction proteins and mucosal adaptive immunity, as well as suppressing the level of inflammation and oxidative stress[53]. All above series of cascade reactions indicate that

the regulation of arginine-proline metabolism has the potential to be a significant target for future prevention of intestinal barrier dysfunction and thus showing positive effects on the treatment of AP.

However, this study has some limitations, including small sample size and lack of clinical validation, thus further studies with enlarged sample size and clinical investigation should be carried out to confirm our findings. Moreover, specific animal and cell experiments are warranted to validate the effect of targeted flora and metabolites in AP. Besides, this study focused on the acute phase of AP, whereas for better analysis, future studies should conduct longitudinal observations and investigate potential dynamic changes in the gut microbiota throughout the overall course of AP.

Overall, this study aimed to evaluate the levels of gut microbiome and serum metabolites in different AP mouse models to determine the function of gut flora-derived metabolites. Interestingly, we found that the composition of gut microbiota and metabolites in the three AP models altered significantly in comparison to the Control group, and the trend of change showed unique performance among different models. Besides, analysis of different strains and metabolite functions mainly involved the abnormal pathways of lipid metabolism and amino acid metabolism. Moreover, *Burkholderiales bacterium* YL45 and *Bifidobacterium pseudolongum* as the main intestinal bacteria appeared to be a reasonable choice to improve the inflammatory responses of AP. Also as expected, targeting gut microbiota and derived metabolites may be a promising avenue for novel treatment development.

Material and methods

Animal experiments and ethical approval

Male *C57BL/6 J* mice (aged 7 weeks and weighing 20–25 g) were provided by the Department of Zoology, Central South University. The mice were housed under specific-pathogen-free (SPF) conditions with free ad libitum access to food and water and maintained in a regular 12 h light–dark cycle. A total of three AP mouse models were employed in the experiments, in which the Caerulein group was induced by hourly intraperitoneal (i.p.) injection of caerulein (200 μg/kg, once an hour for a total of 10 times) (MedChemExpress, USA), and the Caerulein + LPS group was administered by hourly i.p. injection of caerulein (200 μg/kg, once an hour for a total of 10 times) (MedChemExpress, USA) combined with a dose of 5 mg/kg lipopolysaccharide (LPS) (Sigma-Aldrich, USA), mice in the L-arginine group received 2 times i.p. injection of L-arginine (4 g/kg, once an hour, twice in total) (Sigma-Aldrich, USA). Similar saline injections were applied in the Control group. Mice in the Caerulein group, Caerulein + LPS group, and Control group were sacrificed 12 h after the first caerulein or saline injection, while those in the L-arginine group were executed at 72 h. After that, pancreatic tissues were isolated, also blood and feces were collected for further analysis. All animal experimental protocols were approved by the Ethics Committee of Central South University (No. FORM-IACUC-01–01) before the experiments. All the experimental operations were performed in accordance with relevant regulations and ARRIVE guidelines.

Measurement of serum enzymes and pro-inflammatory cytokines

Serum was obtained by centrifuging the blood samples at 3000 rpm for 20 min at a temperature of 4 °C. Serum amylase, lipase, and IL-1β, IL-6, and TNF-α levels were detected using commercial kits purchased from ZCIBIO Technology Co., Ltd. (Shanghai, China) as detailed procedures followed the manufacturer's protocol.

Histological analysis and immunohistochemistry (IHC)

To carry out the histologic evaluation of hematoxylin–eosin staining, the dissected pancreatic tissues were fixed, dehydrated, and then embedded in paraffin. Thereafter, the embedded paraffin sections were cut to a thickness of 3 μm and followed by being stained with hematoxylin and eosin (H&E). For IHC assays, the paraffin sections were dewaxed, endogenous enzymes inactivated and antigens thermally repaired. The sections were then blocked and stained with CD68 or Ly6G antibodies, followed by staining with the appropriate secondary antibodies and hematoxylin. Subsequently, the morphology and structure of the stained sections were observed using a Zeiss microscope. Pancreatic histologic scores were calculated in the aspects of edema, inflammation, hemorrhage, and necrosis as described previously.

RNA isolation and quantitative real-time PCR

According to the instructions of the manufacturer, RNA was meticulously extracted from the colon tissues using TRIzol (Vazyme). Then, we employed the cDNA Synthesis Kit from Vazyme (RC323-01) to conduct the reverse transcription and then performed real-time PCR analysis with ChamQ Universal SYBR qPCR Master Mix, also provided by Vazyme (Q711-02/03). To ensure accurate calibration, β-actin was selected as the internal control to calibrate the original mRNA expression levels. All sequences of primer used in this research are listed in Table S2.

Western blot analysis

The colon was cryogenically ground in liquid nitrogen and lysed in RIPA buffer supplemented with protease and phosphatase inhibitors. The protein concentration in the colon was measured using a BCA protein kit (Beyotime, China). After heating at 100 °C for 10 min, equal amounts of protein were separated by SDS-PAGE and then transferred onto a PVDF membrane. The PVDF membrane was incubated in 5% bovine serum albumin for 2 h at room temperature to seal the non-specifically binding proteins, incubated overnight at 4 °C with primary antibodies, and finally with secondary antibodies incubated for 1 h at room temperature. All antibodies used were purchased from Proteintech Group, China. The protein bands were visualized by electrochemiluminescence (ECL) assay kit (Beyotime, China) and then analyzed the density using Image Lab. Relative protein levels were standardized to the β-actin.

Metagenomics

Fresh fecal samples were collected from mice and immediately frozen in liquid nitrogen. DNA extraction was performed using the CommaXP® Fecal Genomic DNA Extraction Kit, and sequencing was conducted using the MGISEQ-2000 sequencer (MGI Tech Co., Ltd.). To ensure the accuracy and reliability of the data, KneadData software (v0.10.0, https://huttenhower.sph.harvard.edu/kneaddata/) was used for quality control (QC). Briefly, the software employed fastqc for QC, then trimmomatic for filtering, bowtie2 to compare the host genome to remove the host, and finally fastqc to perform QC again. The entire valid sequences of all samples were annotated and categorized by Kraken2 (v2.0.8-beta). Information on species abundance at each level was obtained by comparing CleanData with species sequences in the database. The alpha diversity indices were calculated to analyze the complexity of the species diversity, including the Chao1 index, Shannon index, and Simpson index by using the vegan package from R software (version 2.15.3). Then, analysis of similarities (ANOISM) was analyzed using the anoism function of the vegan package. Distances were calculated using the vegan package and then analyzed by PCoA using the cmdscale. Analysis of composition of microbiomes (ANCOM) was employed to identify the relevant bacteria in each model using the ANCOMBC package. Also, the different groups were assessed regarding the variation in the abundance of microbiota by Linear discriminant analysis effect size (LEfSe) and then visualized with histogram plots. Analysis of metabolic pathways presented in the microbiome was performed using HUMAnN2.

Untargeted metabolomics

50 µL of serum sample was pipetted into an EP tube, mixed with 150 µL of extraction solution (methanol/acetonitrile = 1:1(v/v) containing isotope-labeled internal standard mixture) to separate metabolites. Mass spectrometry analysis was performed using a Vanquish (Thermo Fisher Scientific) ultra-performance liquid chromatograph in positive and negative mode. Quality control (QC) samples were used to ensure stability and reproducibility. Raw data were converted to mzXML format by ProteoWizard software (v3.0.24054-2352758 (automated build), https://hub.docker.com/r/proteowizard/pwiz-skyline-i-agree-to-the-vendor-licenses/tags?page=1&page_size=&name=&ordering=/), processed for peak identification, peak extraction, peak alignment, and integration, and then matched with BiotreeDB (V2.1) self-constructed secondary mass spectrometry database for substance annotation. The final dataset containing peak number, sample name, and normalized peak area information was imported into the SIMCA16.0.2 software package (Sartorius Stedim Data Analytics AB, Umea, Sweden) for multivariate analysis. The R package MetaboAnalystR was used for principal component analysis (PCA), and orthogonal partial least squares discriminant analysis (OPLS-DA). To check the robustness and predictive ability of the OPLS-DA model, 200 permutations were further conducted. Variable Importance in the Projection (VIP) of the first principal component in OPLS-DA analysis was also acquired. Metabolites with $VIP > 1$ and $P < 0.05$ were considered significantly altered metabolites. MetaboAnalyst and KEGG were used for further pathway analysis.

Statistical analysis

All data were statistically analyzed using GraphPad Prism 9.0 software. As for two independent samples, the Student's t test was used for analysis for those who conformed to normal distribution, otherwise Mann–Whitney U test was used. In the comparison of multiple groups, One-Way ANOVA analysis was applied for those that conformed to normal distribution and homogeneity of variance, otherwise Kruskal–Wallis analysis was used. Dunnett's t-test test was processed for two-by-two comparisons. P-values and correlation coefficients between differential bacteria and metabolites were calculated separately using spearman correlation analysis. Threshold at $P < 0.05$ and correlation coefficients > 0.8 were described in the microbiome-metabolite correlations. $P < 0.05$ was considered statistically significant.

Data availability

The datasets generated and/or analysed during the current study are available in the EMBL-EBI MetaboLights database with the identifier MTBLS10760 and the NCBI Sequence Read Archive database in the BioProject with the identifier PRJNA1141391.

Received: 21 April 2024; Accepted: 3 September 2024
Published online: 14 September 2024

References

1. Frossard, J. L., Steer, M. L. & Pastor, C. M. Acute pancreatitis. *Lancet* **371**, 143–152. https://doi.org/10.1016/S0140-6736(08)60107-5 (2008).
2. Xu, F. *et al.* The role of gut microbiota and genetic susceptibility in the pathogenesis of pancreatitis. *Gut Liver* **16**, 686–696. https://doi.org/10.5009/gnl210362 (2022).
3. Yasuda, T. *et al.* Breakdown of intestinal mucosa via accelerated apoptosis increases intestinal permeability in experimental severe acute pancreatitis. *J. Surg. Res.* **135**, 18–26. https://doi.org/10.1016/j.jss.2006.02.050 (2006).
4. Tan, C. *et al.* Dysbiosis of intestinal microbiota associated with inflammation involved in the progression of acute pancreatitis. *Pancreas* **44**, 868–875. https://doi.org/10.1097/MPA.0000000000000355 (2015).
5. Van Felius, I. D. *et al.* Interdigestive small bowel motility and duodenal bacterial overgrowth in experimental acute pancreatitis. *Neurogastroenterol. Motil.* **15**, 267–276. https://doi.org/10.1046/j.1365-2982.2003.00410.x (2003).
6. Wu, L. M., Sankaran, S. J., Plank, L. D., Windsor, J. A. & Petrov, M. S. Meta-analysis of gut barrier dysfunction in patients with acute pancreatitis. *Br. J. Surg.* **101**, 1644–1656. https://doi.org/10.1002/bjs.9665 (2014).
7. Yu, S. *et al.* Identification of dysfunctional gut microbiota through rectal swab in patients with different severity of acute pancreatitis. *Dig. Dis. Sci.* **65**, 3223–3237. https://doi.org/10.1007/s10620-020-06061-4 (2020).

8. Zhu, Y. *et al.* Gut microbiota dysbiosis worsens the severity of acute pancreatitis in patients and mice. *J. Gastroenterol.* **54**, 347–358. https://doi.org/10.1007/s00535-018-1529-0 (2019).
9. Ye, S. H., Siddle, K. J., Park, D. J. & Sabeti, P. C. Benchmarking metagenomics tools for taxonomic classification. *Cell* **178**, 779–794. https://doi.org/10.1016/j.cell.2019.07.010 (2019).
10. Gong, L., Song, X., Su, L. & Wu, D. The research progress on gut microbiota in acute pancreatitis. *Chin. J. Clin. Nutr.* https://doi.org/10.3760/cma.j.cn115822-20210901-00171 (2021).
11. Zhang, C. *et al.* The interaction of microbiome and pancreas in acute pancreatitis. *Biomolecules* **14**, 59. https://doi.org/10.3390/biom14010059 (2023).
12. Krautkramer, K. A., Fan, J. & Backhed, F. Gut microbial metabolites as multi-kingdom intermediates. *Nat. Rev. Microbiol.* **19**, 77–94. https://doi.org/10.1038/s41579-020-0438-4 (2021).
13. Zhao, H. B., Jia, L., Yan, Q. Q., Deng, Q. & Wei, B. Effect of clostridium butyricum and butyrate on intestinal barrier functions: Study of a rat model of severe acute pancreatitis with intra-abdominal hypertension. *Front. Physiol.* **11**, 561061. https://doi.org/10.3389/fphys.2020.561061 (2020).
14. Tran, Q. T. *et al.* Systemic bile acids affect the severity of acute pancreatitis in mice depending on their hydrophobicity and the disease pathogenesis. *Int. J. Mol. Sci.* **23**, 13592. https://doi.org/10.3390/ijms232113592 (2022).
15. Kanehisa, M. & Goto, S. KEGG: Kyoto encyclopedia of genes and genomes. *Nucleic Acids Res.* **28**, 27–30. https://doi.org/10.1093/nar/28.1.27 (2000).
16. Kanehisa, M. Toward understanding the origin and evolution of cellular organisms. *Protein Sci.* **28**, 1947–1951. https://doi.org/10.1002/pro.3715 (2019).
17. Kanehisa, M., Furumichi, M., Sato, Y., Kawashima, M. & Ishiguro-Watanabe, M. KEGG for taxonomy-based analysis of pathways and genomes. *Nucleic Acids Res.* **51**, D587–D592. https://doi.org/10.1093/nar/gkac963 (2023).
18. Silva-Vaz, P. *et al.* Murine models of acute pancreatitis: A critical appraisal of clinical relevance. *Int. J. Mol. Sci.* **20**, 2794. https://doi.org/10.3390/ijms20112794 (2019).
19. Wu, X. *et al.* Emodin ameliorates acute pancreatitis-associated lung injury through inhibiting the alveolar macrophages pyroptosis. *Front. Pharmacol.* **13**, 873053. https://doi.org/10.3389/fphar.2022.873053 (2022).
20. Zhan, X., Wang, F., Bi, Y. & Ji, B. Animal models of gastrointestinal and liver diseases. Animal models of acute and chronic pancreatitis. *Am. J. Physiol. Gastrointest. Liver Physiol.* **311**, G343-355. https://doi.org/10.1152/ajpgi.00372.2015 (2016).
21. Ming-yi, Z., Wen-lü, S. & Chun-qi, X. The rat model of fulminate acute pancreatitis induced by L-arginine. *Chin. J. Exp. Surg.* https://doi.org/10.3321/j.issn:1001-9030.2008.12.045 (2008).
22. Hegyi, P. *et al.* L-arginine-induced experimental pancreatitis. *World J. Gastroenterol.* **10**, 2003–2009. https://doi.org/10.3748/wjg.v10.i14.2003 (2004).
23. Dawra, R. *et al.* Development of a new mouse model of acute pancreatitis induced by administration of L-arginine. *Am. J. Physiol. Gastrointest. Liver Physiol.* **292**, G1009-1018. https://doi.org/10.1152/ajpgi.00167.2006 (2007).
24. Li, Q. *et al.* Bacteremia in patients with acute pancreatitis as revealed by 16S ribosomal RNA gene-based techniques*. *Crit. Care Med.* **41**, 1938–1950. https://doi.org/10.1097/CCM.0b013e31828a3dba (2013).
25. Li, X. Y., He, C., Zhu, Y. & Lu, N. H. Role of gut microbiota on intestinal barrier function in acute pancreatitis. *World J. Gastroenterol.* **26**, 2187–2193. https://doi.org/10.3748/wjg.v26.i18.2187 (2020).
26. Zhu, Y., Mei, Q., Fu, Y. & Zeng, Y. Alteration of gut microbiota in acute pancreatitis and associated therapeutic strategies. *Biomed. Pharmacother.* **141**, 111850. https://doi.org/10.1016/j.biopha.2021.111850 (2021).
27. Patel, B. K. *et al.* Gut microbiome in acute pancreatitis: A review based on current literature. *World J. Gastroenterol.* **27**, 5019–5036. https://doi.org/10.3748/wjg.v27.i30.5019 (2021).
28. Gesualdo, M. *et al.* Pancreatic diseases and microbiota: A literature review and future perspectives. *J. Clin. Med.* https://doi.org/10.3390/jcm9113535 (2020).
29. Frank, D. N. *et al.* Molecular-phylogenetic characterization of microbial community imbalances in human inflammatory bowel diseases. *Proc. Natl. Acad. Sci. U. S. A.* **104**, 13780–13785. https://doi.org/10.1073/pnas.0706625104 (2007).
30. Li, S. *et al.* Salt-sensitive ileal microbiota plays a role in atrial natriuretic peptide deficiency-induced cardiac injury. *Nutrients* https://doi.org/10.3390/nu14153129 (2022).
31. Peterson, D. A., Frank, D. N., Pace, N. R. & Gordon, J. I. Metagenomic approaches for defining the pathogenesis of inflammatory bowel diseases. *Cell Host Microbe* **3**, 417–427. https://doi.org/10.1016/j.chom.2008.05.001 (2008).
32. Song, Q. *et al.* Bifidobacterium pseudolongum-generated acetate suppresses non-alcoholic fatty liver disease-associated hepatocellular carcinoma. *J. Hepatol.* **79**, 1352–1365. https://doi.org/10.1016/j.jhep.2023.07.005 (2023).
33. Zhang, Q. *et al.* Influenza infection elicits an expansion of gut population of endogenous Bifidobacterium animalis which protects mice against infection. *Genome Biol.* **21**, 99. https://doi.org/10.1186/s13059-020-02007-1 (2020).
34. Niu, J. *et al.* Microbiota-derived acetate enhances host antiviral response via NLRP3. *Nat. Commun.* **14**, 642. https://doi.org/10.1038/s41467-023-36323-4 (2023).
35. Ahn, Y. J., Lim, J. W. & Kim, H. Docosahexaenoic acid induces expression of NAD(P)H: Quinone oxidoreductase and heme oxygenase-1 through activation of Nrf2 in cerulein-stimulated pancreatic acinar cells. *Antioxidants (Basel)* https://doi.org/10.3390/antiox9111084 (2020).
36. Jeong, Y. K. & Kim, H. A mini-review on the effect of docosahexaenoic acid (DHA) on cerulein-induced and hypertriglyceridemic acute pancreatitis. *Int. J. Mol. Sci.* https://doi.org/10.3390/ijms18112239 (2017).
37. Chang, Y. T., Chang, M. C., Tung, C. C., Wei, S. C. & Wong, J. M. Distinctive roles of unsaturated and saturated fatty acids in hyperlipidemic pancreatitis. *World J. Gastroenterol.* **21**, 9534–9543. https://doi.org/10.3748/wjg.v21.i32.9534 (2015).
38. Berdel, W. E. *et al.* Ether lipid derivatives: antineoplastic activity in vitro and the structure-activity relationship. *Lipids* **21**, 301–304. https://doi.org/10.1007/BF02536417 (1986).
39. Yao, H. Y. & Xue, H. W. Phosphatidic acid plays key roles regulating plant development and stress responses. *J. Integr. Plant Biol.* **60**, 851–863. https://doi.org/10.1111/jipb.12655 (2018).
40. Hung, N. D., Sok, D. E. & Kim, M. R. Prevention of 1-palmitoyl lysophosphatidylcholine-induced inflammation by polyunsaturated acyl lysophosphatidylcholine. *Inflamm. Res.* **61**, 473–483. https://doi.org/10.1007/s00011-012-0434-x (2012).
41. Sztefko, K. & Panek, J. Serum free fatty acid concentration in patients with acute pancreatitis. *Pancreatology* **1**, 230–236. https://doi.org/10.1159/000055816 (2001).
42. Liu, P. *et al.* The mechanisms of lysophosphatidylcholine in the development of diseases. *Life Sci.* **247**, 117443. https://doi.org/10.1016/j.lfs.2020.117443 (2020).
43. Ceyhan, G. O. *et al.* Prophylactic glycine administration attenuates pancreatic damage and inflammation in experimental acute pancreatitis. *Pancreatology* **11**, 57–67. https://doi.org/10.1159/000325972 (2011).
44. Al-Malki, A. L. Suppression of acute pancreatitis by L-lysine in mice. *BMC Complement Altern. Med.* **15**, 193. https://doi.org/10.1186/s12906-015-0729-x (2015).
45. Ma, C. *et al.* Metabolic characteristics of acute necrotizing pancreatitis and chronic pancreatitis. *Mol. Med. Rep.* **6**, 57–62. https://doi.org/10.3892/mmr.2012.881 (2012).
46. Manoli, I. & Venditti, C. P. Disorders of branched chain amino acid metabolism. *Transl. Sci. Rare Dis.* **1**, 91–110. https://doi.org/10.3233/TRD-160009 (2016).

47. Ye, S. *et al.* Understanding the effects of metabolites on the gut microbiome and severe acute pancreatitis. *Biomed. Res. Int.* **2021**, 1516855. https://doi.org/10.1155/2021/1516855 (2021).
48. Blachier, F., Andriamihaja, M. & Blais, A. Sulfur-containing amino acids and lipid metabolism. *J. Nutr.* **150**, 2524S-2531S. https://doi.org/10.1093/jn/nxaa243 (2020).
49. Rius-Perez, S. *et al.* Blockade of the trans-sulfuration pathway in acute pancreatitis due to nitration of cystathionine beta-synthase. *Redox Biol.* **28**, 101324. https://doi.org/10.1016/j.redox.2019.101324 (2020).
50. Rahman, S. H., Srinivasan, A. R. & Nicolaou, A. Transsulfuration pathway defects and increased glutathione degradation in severe acute pancreatitis. *Dig. Dis. Sci.* **54**, 675–682. https://doi.org/10.1007/s10620-008-0382-z (2009).
51. Brandt, A. *et al.* Impairments of intestinal arginine and NO metabolisms trigger aging-associated intestinal barrier dysfunction and "inflammaging". *Redox Biol.* **58**, 102528. https://doi.org/10.1016/j.redox.2022.102528 (2022).
52. Li, J. *et al.* VSIG4 inhibits proinflammatory macrophage activation by reprogramming mitochondrial pyruvate metabolism. *Nat. Commun.* **8**, 1322. https://doi.org/10.1038/s41467-017-01327-4 (2017).
53. Satriano, J. Arginine pathways and the inflammatory response: Interregulation of nitric oxide and polyamines: Review article. *Amino Acids* **26**, 321–329. https://doi.org/10.1007/s00726-004-0078-4 (2004).

Acknowledgements

The author would like to thank the Hunan Yearth Biotechnological Co., Ltd and Shanghai Biotree Biotech Co., Ltd for providing metagenomics and metabolomics sequencing technologies. This study was funded by the National Natural Science Foundation of China (Grant No. 82170661), the Key Project of Research and Development Plan of Hunan Province (Grant No. 2023DK2002), the Postdoctoral Fellowship Program of CPSF (Grant No. GZC20242045), and the Fundamental Research Funds for the Central Universities of Central South University (Grant No. 2023zzts896).

Author contributions

J.P., Y.J., and Y.X.S. proposed the conception and designed the experiments. Y.J., Y.X.S., and J.W. performed all of the experiments and wrote the main manuscript. H.H.L. and Y.L.H. analyzed the data. H.Y.W. and Y.L. prepared the figures and revised the manuscript. All authors reviewed and approved the final submitted manuscript.

Competing interests

The authors declare no competing interests.

Additional information

Supplementary Information The online version contains supplementary material available at https://doi.org/10.1038/s41598-024-72057-z.

Correspondence and requests for materials should be addressed to J.P.